CONSTRUCTION AND TESTING OF A Cd - PHOTOIONIZATION LASER

Diploma Paper

Björn Bengtsson & Frederik Ossler

Department of Physics
Lund Institute of Technology
LRAP - 61

Lund Reports on Atomic Physics
LRAP - 61

PREFACE

This is a diploma work made at the Department of Atomic Physics at Lund Institute of Technology. The purpose of this project was to construct and test a VUV laser working by the principle of photoionization.

Because of the practical problems arising when it comes to maintaining a desirable metal vapour pressure and keeping the temperature reasonably low the choice of cadmium as ionization medium is natural.

A very important factor with any substance used for this type of laser is the shape of the photoionization cross section. It is also of great importance to have access to a pumping source with enough energy to produce a radiating plasma from an irradiated target with suitable characteristics. The plasma temperature must correspond to the peak of the photoionization cross section of the ionization medium. With the use of a Nd:YAG laser and a tungsten target we managed to create a working VUV photoionization laser.

In order to make the report more easily read all calculations have been put in separate appendices, but all results of any importance are presented in the text.

We would like to thank our supervisor Dr. Hans Lundberg for his invaluable help in outlining and conducting this work.

LUND, MAY 1986

Björn Bengtsson

Frederik Ossler

CONTENTS

1 INTRODUCTION

During the last ten years or so much effort has been put into finding ways of producing short wavelength lasing systems. Knowledge of methods of achieving coherent X-ray radiation could revolutionize and open new fields within medicine (microsurgery, genetics), chemistry, biology (microscopy, gene manipulation), high-tech industry (photolitography). One should however not forget the political and military aspects as in the case of "star wars".

In spectroscopical applications, it has been possible to do studies of excited states in the VUV and XUV spectral regions, with coherent and narrow line width VUV radiation generated with laboratory scale dye laser systems. Powers as high as 10kW/pulse have been produced within the region of 100 to 200nm[ref 1]. The corresponding power from synchrotron radiation is about 10^{17} lower. Through a sequence of harmonic generation steps of higher order (>2) nonlinear processes, tunable radiation has been produced in the region of 60 to 80 nm with dye lasers. Visible light is converted to wavelengths as short as 20 nm with anti-Stokes scattering from metastable species. Studies of the spectroscopy and dynamics of excited states in the VUV are often carried out by means of multi- photon absorption, multiphoton ionization, harmonic genaration and laser assisted energy transfer. VUV- lasers can be divided into two categories:

1) The levels are excited in a travelling wave configuration where the optical emission closely follows the excitation pulse, as the latter propagates through the laser medium ,so that no optical cavity is required . This group consists of low - pressure, gas discharge type lasers,using small molecules such as CO, H_2,HD, or D_2. There is no phase coherence in the output, and they give nothing but amplified spontaneous emission.

2) Usage of an optical cavity is necessary for operating purposes. The most common contributers are the excimer lasers of the rare gases. Excitation is performed by an electron beam pump to produce excimers (Xe_2* , Kr_2* , Ar_2*) or by a high- pressure preionized discharge to generate exciplexes (ArF*) as the upper level.

A more recent method of producing coherent short wavelength radiation has sprung up. It has been shown mainly from theoretical work but recently also from practical work that photoionization due to blackbody radiation from laser plasmas in the X- ray region shows good overlap with inner shell photoionization for several species of free atoms[ref 2,3]. Metastable levels of the ionized atomic system are thus produced with a high population inversion compared to the lower level, in the lasing process, which belongs to a less ionized atomic system. VUV and XUV radiation of sufficient intensity for laser applications is then produced. One of the initial steps in trying to study these principles of radiation is perhaps taken in the studies on the Cd- photoionization laser operating in the 4416 Å (and 3250 Å).

2 THEORETICAL BACKGROUND

2.1 PHOTOIONIZATION OF CADMIUM

In this text we will often refer to the atomic system of Xe,when discussing the photoionization cross section of Cd, because of the richer reference of the former. However both elements have similar electronic configuration with filled subshells and the difference consists of that Xe has additional six 5p orbitals filled, so the general form of the photoinization cross section for 4d subshell ionization of cadmium, seen from figure 2.1, as a function of energy should resemble that of xenon. Small deviation can be seen just below 30 Å for Cd, where the contribution from another subshell becomes dominant.

Fig 2.1 a).

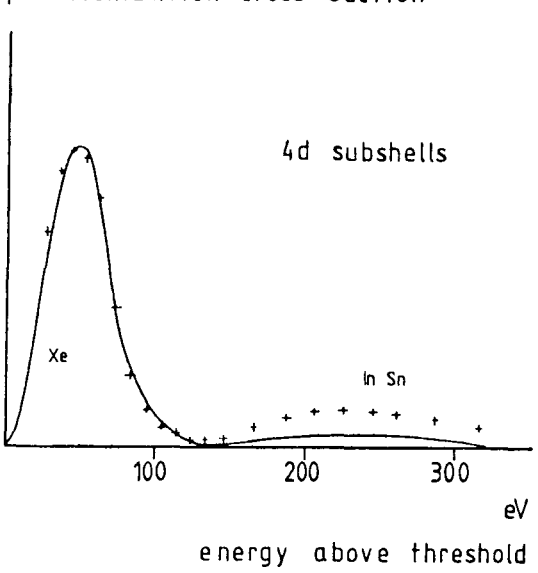

Fig 2.1 b).

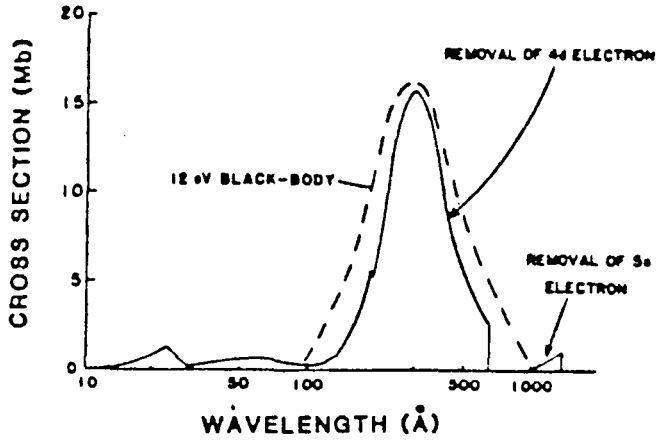

Fig 2.1 a). Relative photoemission cross sections of the 4d subshell for solid tin and indium compared after normalization with theoretical(solid curve) free atom 4d results on xenon.

Fig 2.1 b). Photoionization cross section versus wavelength for Cd-vapour. The dashed curve shows the emission spectrum of a 12 eV blackbody.

The photoionization cross section of Xe and Cd due to 4d subshell photoionization can be calculated with results which in a high degree are in agreement with experimental results[ref 4]. Let us start with a simple description.

$$\nu + X_i \rightarrow X_j + e \qquad (2.1)$$

ν = photon impinging on a neutral system in state i

X_i = initial state

X_j = final state of the singly charged system

e = free electron

$$E_e = h\nu - I_{ij} \qquad (2.2)$$

E_e = photoelectron energy

I_{ij} = energy required to move an electron from X_i to X_j without giving it kinetic energy

For an atom we can deduce the cross section for photoionization in the dipole approximation.

$$\sigma(\nu) = 4/3\ \pi^2\ e^2 |\langle\psi_j| \sum_k \bar{r}_k |\psi_i\rangle|^2/hc \qquad (2.3)$$

Where $|\langle\psi_j| \sum_k \bar{r}_k |\psi_i\rangle|^2$ is the dipole moment strength per unit energy

With appropiate approximations the integral:

$\langle\psi_j| \sum_k \bar{r}_k |\ \psi_i\rangle$ is reduced to

$$\int \Phi_0(r)\ \bar{r}\ \Phi_f(r) d\tau. \qquad (2.4)$$

This last expression can be reached with the following assumptions:

(i) The Born - Oppenheimer approximation.

(ii) The electronic wave functions ψ_0 and ψ_f are antisymmetrized products of one electron wave functions.

(iii) in the central field approximation ,There are n-1 identical one electron wave functions in the expression for ψ_0 and ψ_f equal to one in the integral . Relaxation of the ion core during the ionization process is then neglected.

(iv) Since we are looking at the central symmetric solutions the one electron wave functions are separable in radial and angular coordinates (spin is ignored), $\Phi(r)$ are thus interpreted as radial functions.

We have now ψ:s that could be exact solutions to central potential - Hamiltonians.

If we look at electronic transitions from d-subshells, we can see that electric dipole selection rules require final states in p or f shells for one electron transitions. However it can be shown that transitions to the greater ℓ-value are more probable [ref 5]. The number of radial nodes in the initial state shows to be of great importance when discussing photoionization. Cooper [ref 5] was the first to take up this subject in saying that photoionizatation cross section for photionization processes from subshells with no radial nodes have no zero minima, while others do.

Let $$N=n-(\ell+1) \qquad (2.5)$$

where N=number of radial nodes. This implies that 4d subshell ($n=4, \ell=2$) should have one minimum.

The last integral expression (2.4) for the matrixelement can roughly be regarded as an overlap between the initial 4d and the final εf state, εf representing free electron continuum state.

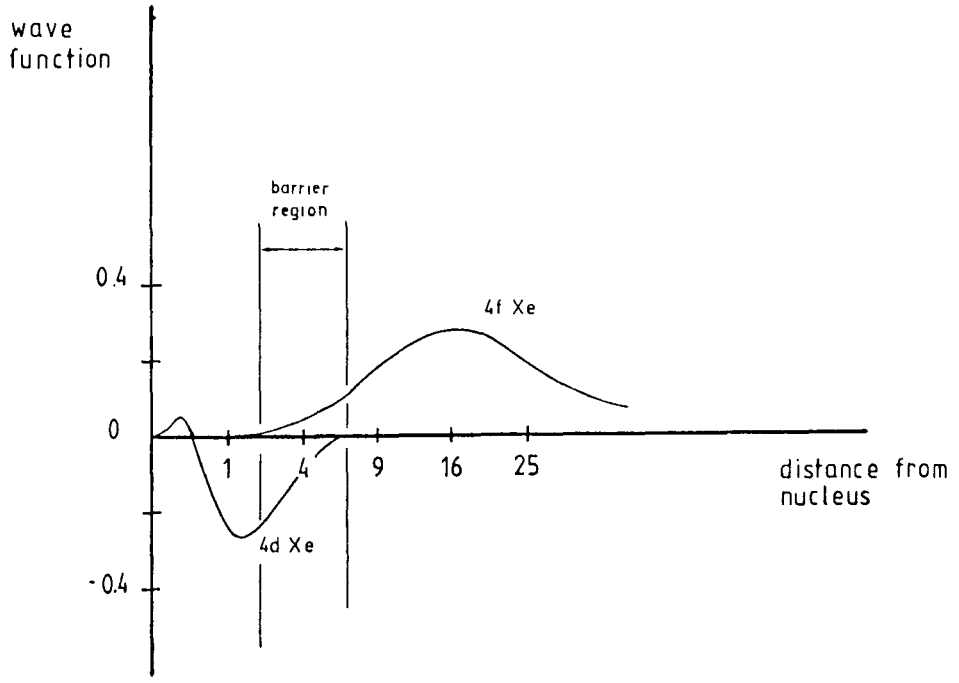

Fig 2.2 Wave function for the 4d and 4f orbitals of xenon.

The radial wavefunctions appearing in expression (2.4) are solutions for the central field Schrödinger equation (in Hartree units)

$$\left[\frac{-d^2}{dr^2} - 2V(r) - 2E + \frac{2\ell(\ell+1)}{r^2} \right] \Phi(r) = 0 \qquad (2.6)$$

With the boundary conditions $V(r) \rightarrow z/r$, $r \rightarrow 0$

and

$V(r) \rightarrow 1/r$, $r \rightarrow \infty$

Let $$Vl = -2V(r) + 2\ell(\ell+1)/r^2 \qquad (2.7)$$

The term $\ell(\ell+1)/r^2$ is the repulsive centrifugal potential.

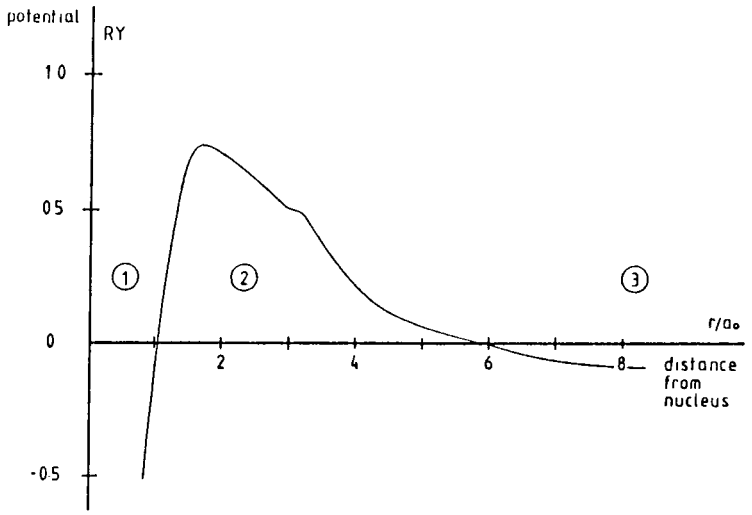

Fig 2.3 The potential Vl as defined in (2.7) for $\ell \geq 3$. The regions represent: (1) Strong Coulomb attraction. (2) Repulsion barrier where the centrifugal term dominates. (3) Weak Coulomb attraction due to the screening effect of the inner filled orbitals. Here the near range centrifugal repulsive term weakens out.

Generally [ref 5] the potential Vl ,for $\ell \geq 3$,has the form of fig 2.3 .

We have in the regions:

(1) Strong Coulomb attraction.

(2) Repulsion barrier where the centrifugal term dominates.

(3) Weak Coulomb attraction due to the screening effect of the inner filled orbitals. Here the near range centrifugal repulsive term weakens out.

In the outer well region we have approximately:

$$Vl = \ell(\ell+1)/r^2 - 2/r \qquad (2.8)$$

The coordinates of the outer well can be given analytically as:

$$r(min) = \ell(\ell+1) \quad \text{in a.u.} \qquad (2.9)$$

$$Vl(r(min)) = -1/2\ell(\ell+1) \qquad [\text{ref } 5] \qquad (2.10)$$

States just below the barrier maximum i.e. valence, Rydberg, and low energy continuum states, are the the most affected by the barrier maximum, meaning that states in this energy region either tend to be eigenfunctions of the inner or outer well.

Let us now turn back to our discussion on cooperminima. In our case we have an inital 4d state with one radial node in our wavefunction. At very low energies , $\varepsilon \approx 0$, we have almost no overlap between the two orbitals in expression (2.4), since the $[\varepsilon f$ is the solution to the outer well potential. But increasing the energy enough (ε is high) the εf wave succeeds in penetrating the barrier, reaching the situation where the first lobe of the εf wave starts to overlap the negative greater one of 4d bound sublevel. This increasing overlap corresponds to an increasing photoionization cross section in which the matrixelement has a negative sign. Continuing our increase in energy of the free electron in its way towards the nucleus, the overlap reaches the positive 4d lobe reducing the negative matrix element to zero. Passing this energy the matrix element starts to increase, not to as high an absolute value as before but to a new lower maximal value, whereafter it decreases to zero again.

So far we have only taken in account the solutions of the central field Schrödinger equation, which however is not the exact description of our system. Terms like exchange forces are then excluded, being mainly non central. Calculations that implement this exchange effect [ref 4] show how the interactions tend to broaden and shift the photoabsorption maximum to higher energies. Also, the first maximum is increased.

At last we should mention something about the relativistic effects that so far have been left out, and which turn out to be of great importance in the description of the photoionization processes of Cd and also of Zn and Hg. These elements share the same valence shell configuration of $nd^{10}(n+1)s^2$. The relativistic effect results in a spin - orbit splitting, which separates the ℓ shell into $\ell \pm 1/2$ subshells. The $\ell+1/2$ wave is somewhat repulsive, while the $\ell-1/2$ is the contrary, compared to the original ℓ- wave. The $\ell+1/2$ has a larger overlap with the continuum wave, while the opposite holds for the $\ell-1/2$. In terms of energy this means that the $\ell+1/2$ leads the $\ell-1/2$ When the partial cross section for ionization is increasing $\ell+1/2$ leads $\ell-1/2$ and when the partial cross section is falling, because of the cancellation of positive and negative parts of the matrixelements, the $\ell+1/2$ will also lead the decline.

This explains why the statistical ratio of 3:2 between $^2D_{5/2}$ and $^2D_{3/2}$ is not achieved. At 584 Å, when the energy of the free electron is rising for Hg, encompassing a rising and falling cross section from ca 2.0 to 1.3 for 584 Å to 256 Å Silfvast and Wood [ref 2] say that Cd has a statistical ratio of 1.6 - 1.7 between 4416 Å and 3250 Å. In fig(2.1) the cross secion for d-electron removal reaches threshold at 700 Å, increases to its maximum value of ca 15 Mbarns at 300 Å, and becomes negligible at 100 Å. 12 eV blackbody emission shows a good overlap with the photoionization cross section, suggesting the black body radiation of corresponding temperature to be used as an effective

photoionization source.

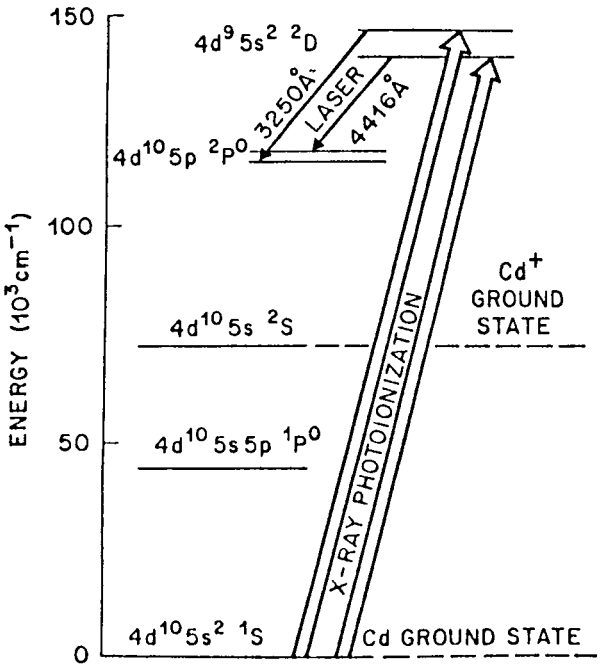

Fig 2.4 Partial energy level diagram of cadmium .

2.2 BLACKBODY RADIATION FROM PLASMAS

As we can see from above blackbody radiation as a pumping source in photoionization lasers emitted by laser induced plasmas from heavy Z-targets turns out to be an effective method to produce highly population-inverted states.

Plasmas are in this case produced by vapourization of some opaqe surface (in our case at the surface of the Tungsten target) and subsequent absorption of laserlight in the vapourized material. The laser light is absorbed at and below the critical density surface which calculations give as 50 to 100µm from the original target surface. Most of the sub - keV X - rays are emitted within 20 µm of the original target surface [ref 6].

The energy available for X- ray emission is reduced by the decrease in electron thermal conductivity since the laser energy must be transported from the overdense plasma to the underdense plasma.Plasma production studies are carried out at high irradiances of 10^9 W/cm^2 or greater [ref 7]. Studies on single species of charged particles on the other hand are preferrably carried out at irradiances of 10^7 to 10^8 W/cm^2.

Plasma produced in the laser-surface interaction show from optical spectroscopic studies both continuum and line radiation. The interesting type of radiation in our case i.e. the continuum type is emitted near the target surface and covers much of the spectral range 20 Å to 6000 Å, whilst the line radiation presenting high ionization stages of ions seems to originate as far out as several centimetres from the target surface.

One interesting parameter of the plasma to be determined was the temperature and a technique to estimate it was through measurements of the monochromatic blackbody temperature from emission intensities of the plasma over a range of wavelengths [ref 7]. There is some difficulty in interpreting the results since the plasma generally is in neither collisional nor radiative equilibrium due to the transient nature of the phenomenon.

An important concept is that of local thermodynamic equilibrium, since the plasma then can be described by a single temperature function. Local thermodynamic equilibrium will hold when collisional excitation and energy transfer processes are sufficiently rapid. Various criteria on the collision times must be satisfied in order to have local thermodynamic equilibrium. The most stringent is generally the time for equalization of electron and ion temperatures. For laser produced plasmas where the electron densities typically are high, the electron-ion collision time may be less than 10^{-9} s. Thus in time scale of conventional Q- switched laser pulses it is possible to achieve local thermodynamic equilibrium. For picosecond pulses this is generally not the case.

The absorption of laserlight in the blowoff material of the target will heat the vapour further in the plasma production process. The electron is raised to higher continuum state through the inverse bremsstrahlung process, which involves absorption of a photon by the free electron. However conservation laws of momentum require the participation of an ion with its electric field. The corresponding absorption coefficient is given in [ref 7]. For T >> 20,000 K as in

our case, it can be approximately expressed as:

$$K_\nu \approx 4/3(2\pi/3)^{0.5}\ (1/mkT)^{1.5}\ (n_e n_i\ Z^2\ e^6/c\nu^2) \quad \text{cgs} \quad (2.11)$$

K_ν = absorpion coefficient in cgs
m = electron mass
k = Boltzman constant
t = absolute temperature of the plasma
n_e, n_i = densities of electrons and ions respectively
Z = average ionic charge
e = electron charge
c = velocity of light
ν = frequency of light

Efficient heating requires the plasma to be of dimension around $1/K_\nu$. If it is less, energy will be lost, and if its more the plasma will not be heated uniformly . In order for the laser energy to penetrate into the plasma the optical frequency must be higher than the plasma frequency ν_p:

$$\nu_p = 8.9 * 10^3\ n_e^{0.5} \quad (2.12)$$

At higher electron densities, the plasma will reflect the radiation and light will not penetrate. The equipartition time for transfer of absorbed energy from electrons to ions can approximately be given as:

$$t_1 \approx 252\ AT^{1.5}/(n_e Z^2)\quad \ln\Lambda \quad (2.13)$$

$\ln\Lambda$ = often the order of 10
A = atomic weight of the ions

In many cases t_1 will be much shorter than the scale time of the Q- switched laser pulse. Thus electron and ion temperatures can be regarded as equal. Radiation from the plasma will be dominated by Bremsstrahlung. The emitted power is:

$$P = 1.42 \cdot 10^{-34}\ Z^3\ n_i^2\ T^{0.5} \quad W/cm^2 \quad (2.14)$$

For many cases of interest the radiated power however is much smaller than the input power. The plasma will radiate like a blackbody only when the absorption length is smaller than the plasma dimensions. Blackbody emission is often negligible below 10^6 K, indicating that in many practical cases radiated power is low, but sufficient for photoionization purposes. To get rates high enogh to be of use, you have to use high Z targets as blackbody emission sources.

The free mean path of the radiation is generally much shorter than the plasma scale length in high Z targets [ref 8] such as Tungsten (Z = 74), inferring the validity of blackbody radiation spectra.

Studies on sub - keV X-ray emission from disk targets illuminated with 1 ns, 1.06 μm wavelength pulses at nominal intensity of $5 \cdot 10^{14}$ W/cm^2 [ref 6] show the existence of an onset of strongly inhibited electrothermal conduction during the rise of the laser intensity. This onset takes place at higher energies for higher Z- materials. The inhibition of electron thermal conduction is caused by self generated magnetic fields, ion acustic turbulance, and electrostatic fields set up by superthermal electrons. Thus one cannot go above a certain optimal level of pumping light intensity.

The dependence in experimental results on parameters such as :

laser intensity
pulse width
wavelength
spot size
target material
beam uniformity

should give good understanding of inhibition process and give the dominant mechanisms.

3 EXPERIMENTAL ARRANGEMENT

The general experimental arrangement used to produce a photoionization laser in cadmium is shown in fig 3.1 .

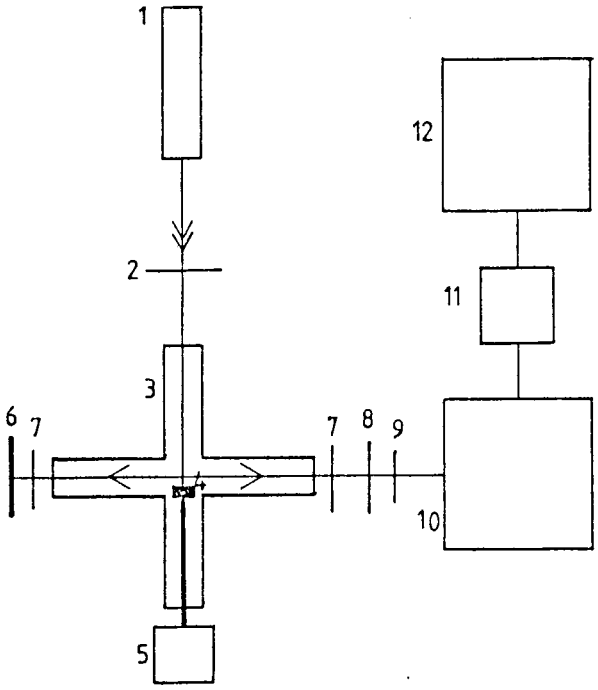

Fig 3.1 *Experimental set-up for photoionization laser diagnostics.*
(1) Nd:YAG Laser
(2) Focusing Lens
(3) Heat Pipe
(4) Tungsten Target
(5) A.C. Engine
(6) End Mirror
(7) Diaphragm
(8) Laser Mirror
(9) Attenuation Filter
(10) Monochromator
(11) Photomultiplier
(12) Oscilloscope.

It consists of a one inch outer diameter heat pipe [ref 9] made of stainless steel tubes welded together in the shape of a cross. All four arms of the cross were coupled with Swagelok tube fittings to blocks made of aluminium. Three of these blocks had windows glued to their ends. On the block pointing against the Nd:YAG laser (see fig 3.1) the window was placed perpendicular to the arm of the cross, but on the other two that were placed on the optical axis of the photoionization laser the windows were put in an angle of 15^{0} to a plane perpendicular to the optical axis. This arrangement was made to prevent reflections in the end-windows from contributing to the measured gain. The fourth block ended with a Swagelok tube fitting through which a steel rod was placed. To one end of the rod there was fitted a holder made of steel. In this holder a piece of tungsten metal that would serve as a target was placed. The tungsten, serving as a target, was put in the central region of the heatpipe. The other end of the rod was coupled to an a.c. engine with the help of a system of gear wheels. Thus the target could be caused to rotate. The speed of rotation was approximately 3 r/min. The reason for the target to be rotated was to prevent it from being too rapidly consumed.

The above mentioned aluminium blocks were also coupled to a system of 6 mm diameter teflon tubings used to evacuate the heat pipe with the help of a vacuum pump. The tube system was also used to lead helium gas into the heat pipe. The helium was used to slow down the cadmium atoms and prevent the cadmium from forming a coating on the inside of the end windows. All Swagelok tube fittings were made vacuum proof with the help of O-ring gaskets and vacuum grease.

The cadmium vapour was obtained by putting a piece of cadmium metal near the centre of the heat pipe. The heat pipe was then heated using a 2.5 m length 640 W heating tape wired around the central parts of the heat pipe so that a temperature gradient in the arms of the heat pipe was obtained (see fig 3.1). The maximum obtainable temperature in the centre was about 850 K using this equipment. The heat pipe was fitted at all ends of the cross with cooling-blocks of brass through which cold water was passed and was thus effectively cooled. The temperature was measured with the use of Fe-constantane thermocouples and a voltmeter.

As shown in fig 3.1 a 1.06 μm laser beam from a Nd:YAG laser was focused with a 35 cm focal length lens onto the tungsten target. The Nd:YAG laser power, which was approximately 50 MW/pulse, thus produced a soft-X-ray source with an approximately 10-15 eV blackbody distribution for the duration of the laser pulse (10 ns). The active length of the medium was about 1 cm.

The resulting laser and gain pulses were detected with a system consisting of a monochromator, a photomultiplier and a fast oscilloscope (risetime 1 ns). Sometimes an oscilloscope camera was used. In measurements of high amplifications, the use of attenuation filters was necessary.

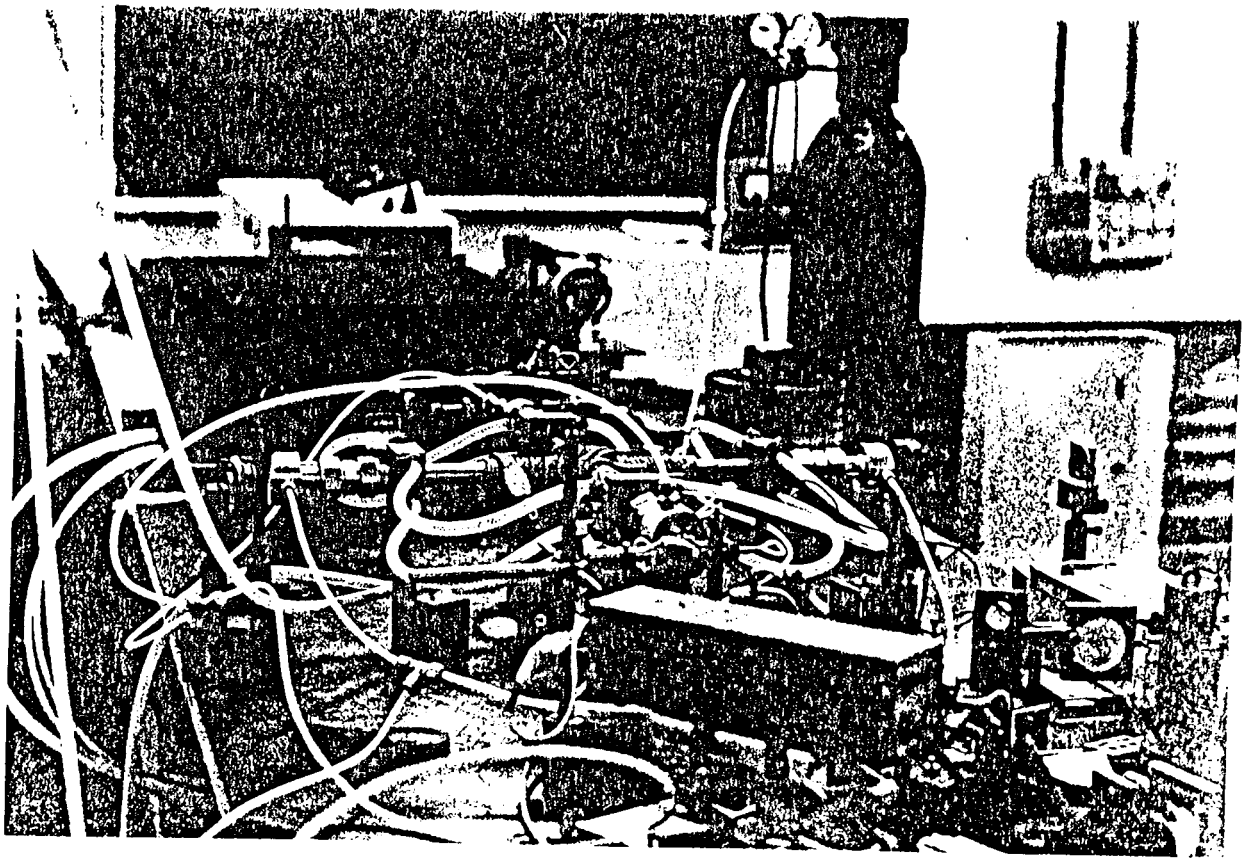

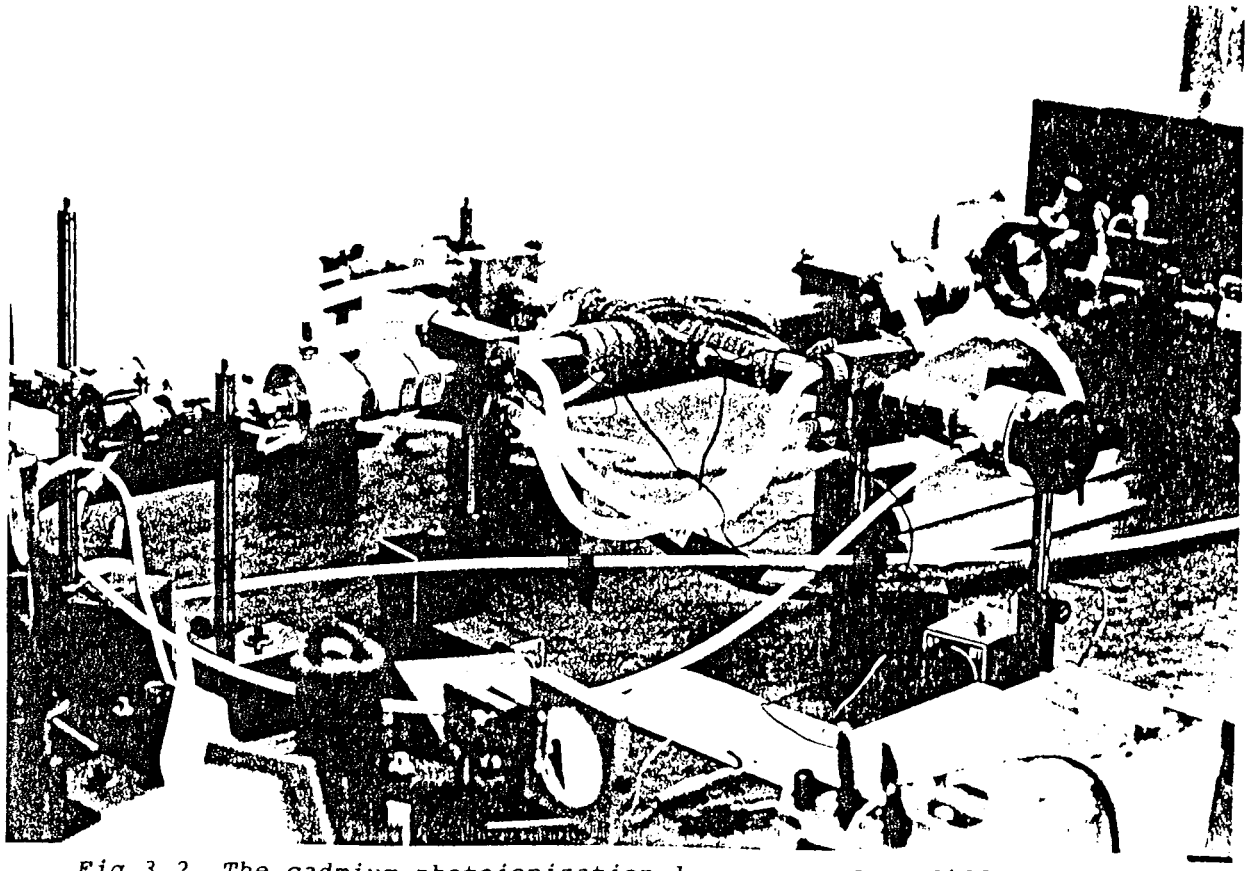

Fig 3.2 *The cadmium photoionization laser seen from different angles.*

4 THE EXPERIMENTS AND RESULTS

4.1 INTRODUCTORY EXPERIMENTS

After constructing the heat pipe the experiment shown in fig (3.1) was set up. The rear mirror was aligned and the pipe heated. At a temperature of about 500 ^{0}C the Nd:YAG laser was turned on. We imediately detected strong gain spikes on the oscilloscope. An out-put coupler was then installed and laser light at 4416 Å was visually observed. In order to optimize and make diagnostics of this photoionization pumped laser a series of experiments was performed. In these experiments the gain was measured. At all measurements diaphragms with an apperture cross section of about 2 mm were placed at both ends of the tube, thus limiting the active volume studied. Before every experiment a He-Ne gaslaser, operating at 6328 Å, was used to simulate the actual photoionization Cd-laser beam, in order to align the system.

Three general methods were used in order to register and determine the gain due to stimulated emission:

1) Measurement of the ratio of emission in the prescence or absence of a mirror placed behind the heat pipe on the optical axis, as shown in fig 3.1 . This was the method most frequently used in the experiments that are described below.

2) Measurement of the enhancement obtained when an optical resonator was placed around the heat pipe. Fig 3.1 .

3) Observation of He-Cd laser light transmited through the heat pipe.

The formula used to compute the gain according to method 1) above is derived in appendix 1).

The object of the first experiment was to determine how the gain is varying with the position of the focusing lens, i.e. the size of the irradiated spot at the target. The helium pressure in the heat pipe was kept at 10 torr. The emission with and without a mirror behind the heat pipe was measured for a number of positions of the lens. The resulting computed gains were then plotted against the position of the lens. The graph is shown in fig 4.1.1 .36 and 41 cm correspond to spot diameters of 202 and 230 µm, respectively.

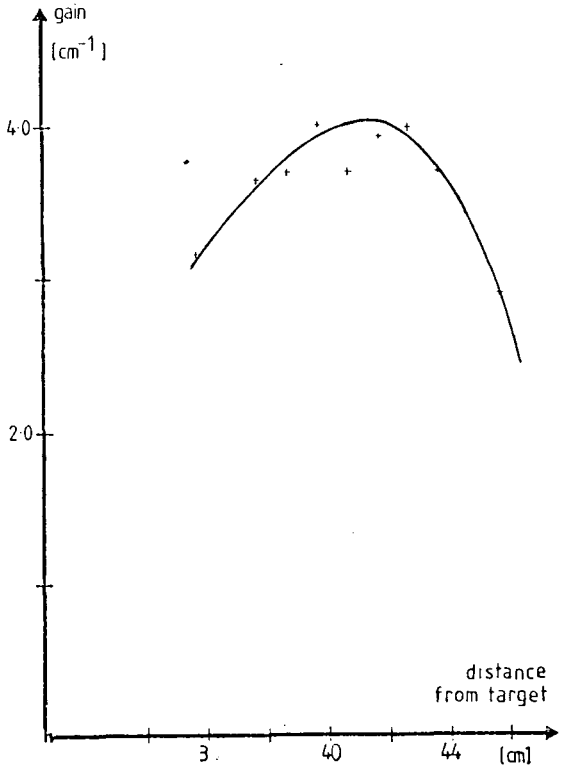

Fig 4.1.1 *Gain as a function of the distance between the focusing lens and the target, i.e. spot size on the target.*

The next experiment aimed at investigating the measured emissions dependance of the Nd:YAG laser pulse energy. The helium pressure was kept at 10 torr. The emission with and without an end mirror was measured for different laser pulse energies, ranging from 0.2 to 0.5 joule. The position of the focusing lens was optimized for every pulse energy, in order to tune the peak of the blackbody radiation to optimum. Results are shown in fig 4.1.2 .

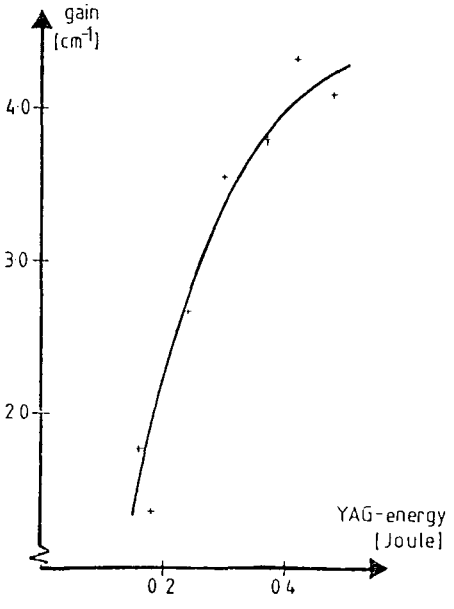

Fig 4.1.2 *Gain as a function of Nd:YAG laser pulse energy.*

The following experiment was a study of how the distance between the tungsten target and the area of measurements, as defined by the diaphragms, affects the gain. In order to do this the target was moved back and forth and the position of the focusing lens was optimized for every measurement. The gain was then determined according to method 1) above. The resulting graph of gain versus position of the target is shown in fig 4.1.3 . Ref[3] explains the lower gains near the target, where a higher gain might be expected due to the higher pumping flux, as resulting from electron collisions thermalizing the upper and lower laser levels. Other possible effects near the target that could lead to a decreased gain are stimulated emission and hot electron penetration from the plasma X-ray source into the surrounding vapour. The reason why the gain is decreasing further from the target is that the X-rays are diverging and thus the pumping flux is reduced.

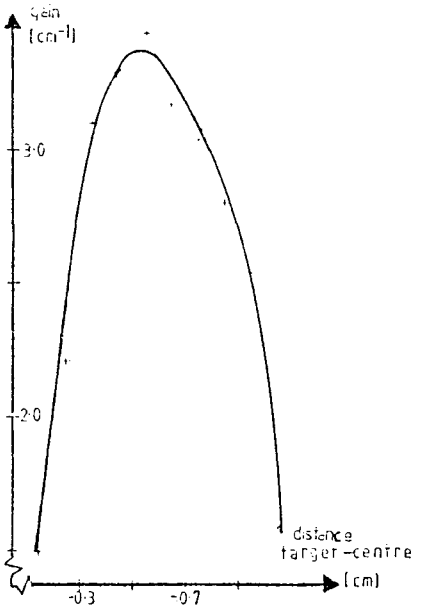

Fig 4.1.3 *Gain as a function of the distance between the target and the centre of the active volume.*

There was also made a study of the gain dependence on the helium pressure. Gain was determined according to method 1) above, and the helium pressure was varied from 20 to 3 torr. The resulting graph is shown in fig 4.1.4 . The reason why the graph flattens out at low helium pressure is that the number of cadmium atoms in the active volume is decreasing.

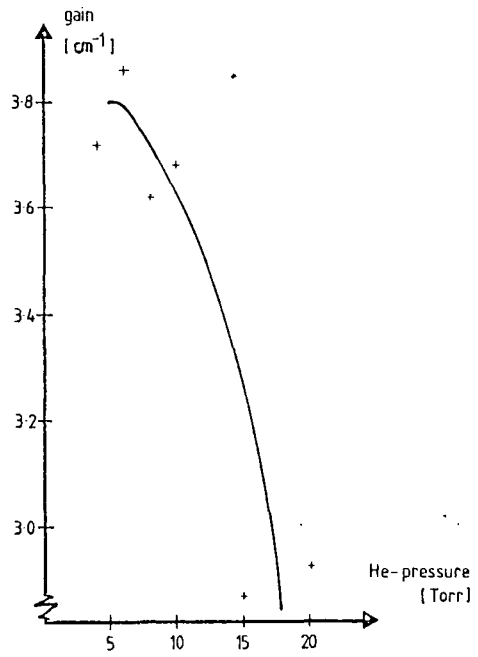

Fig 4.1.4 *Gain as a function of helium pressure.*

With the object of investigating the gain dependence on the density of cadmium atoms in the active volume, a number of measurements of the gain at different temperatures ranging from 710 to 810 K were made. The pressure was kept at 10 torr and the gain was determined by method 1) above. In order to get the atom densities a separate series of measurements had to be made. In these measurements light from a high pressure xenon lamp was sent through the heat pipe and the absorption profile for the transitions $5s5p\ ^1P_1-5s^2\ ^1S_0$, where λ=2289 Å, and $5s5p\ ^3P_1-5s^2\ ^1S_0$, where λ=3262 Å was registered with a monochromator and a plotter. This was made for a number of different temperatures. The atom densities could then be determined with curve-of-growth technique, (described in appendix 2). The resulting gain as a function of atom density is shown in fig 4.1.5 . For calculations see appendix 3.

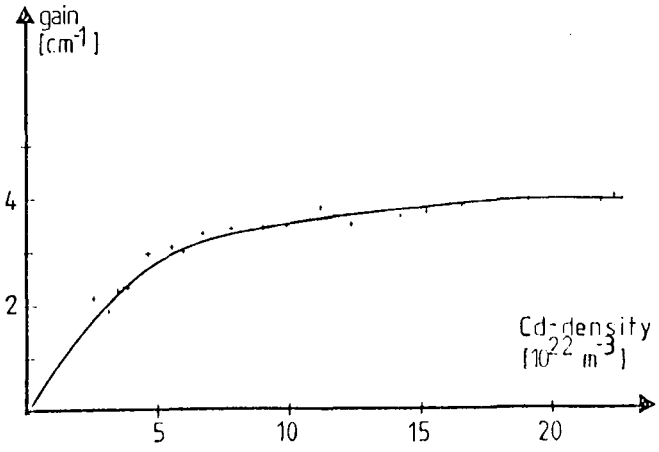

Fig 4.1.5 *Gain as a function of Cd-density.*

An investigation of the time intervals of the Nd:YAG laser pulse, emission (without end mirror),enhanced pulse (with end mirror), and the cadmium photoionization laser pulse was made, and the shape of the pulses were registered on the oscilloscope and photographed with an

oscilloscope camera. Typical pulse shapes are shown in fig 4.1.6 .

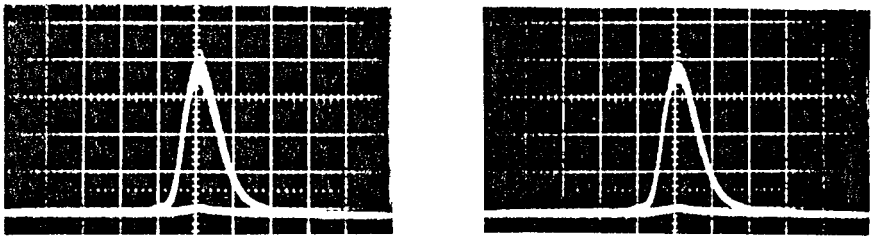

Fig 4.1.6 Gain measurements using the mirror technique for different atomic densities. The peaks correspond to the mirror blocked and unblocked.

4.2 RESULTS ON THE G - FACTOR

The best way of determining the G - factor in our experiments was done by measurements on the radiation from a calibrated He-Cd laser passing through the photoionization - laser. Here we used the 4416 Å line and photographed the amplifiction. The power out from the calibrated probe - laser was given, thus the gain was easily calculated from the photographs.

The maximum amplitude of the amplified radiation was taken from the photographs while the amplitude from direct measurements on the calibrated source was 0,110 in equivalent units. 1 cm active length in the laser in the expressions below gives the following results :

$$\frac{A_A}{A_C} = \frac{\text{Amplitude (amp.)}}{\text{Amplitude (cal.)}} = e^{G\,L} \quad ; \quad L = 0.01 \text{ m}$$

$$G = 1/L * \ln (A_A/A_C)$$

T = 496 ^{0}C G = 100 * ln (7.5/ 0.110)
p = 10 Torr = 420 m^{-1}

T = 518 ^{0}C G = 440 m^{-1}
p = 10 Torr

From the measured gain values the population inversions could be calculated, (see appendix 5):

$$N = 2.1 \cdot 10^{13} \text{ cm}^{-3} \text{ at a temperature of } 500\ ^0\text{C}.$$

The population inversion could also be calculated from the blackbody radiation absorbed in the active volume, (see appendix 4):

$$N = 7.8 \cdot 10^{12} \text{ cm}^{-3} \text{ at a temperature of } 500\ ^0\text{C}.$$

4.3 DATA ON THE Cd-PHOTOIONIZATION LASER

From the photographs taken, several charcteristics of the laser were determined, such as output power, output energy, onset(delays)- and lifetimes of the emitted pulses. The technique used was amplification by mirror technique (blocked/ unblocked rear mirror), and stimulated emission in a resonance cavity, which consisted of a front mirror (8% refl. glass for high emission and 95% mirror for low emission) and an unblocked rear mirror. The data are given below.

Lasing modus 4416 Å

	Output	Pulse energy
Temperature = 580 °C Pressure = 5 Torr No diaphragms glass of 8 % refl.	43 W/ pulse	1.97 µ Joule
With output mirror 95 % refl.	24 W/ pulse	1.09 µ Joule
Temperature = 500 °C 2mm diameter diaph.	4.8 W/ pulse	0.22 µ Joule
Temperature = 580 °C	6.7 W/ pulse	0.31 µ Joule
Temperature = 500 °C Pressure = 10 Torr	1.9 W/ pulse	0.088 µ Joule

Onset and lifetimes of the pulse

Laser onset :	8 ns
pulse-time :	20 ns
Amplification onset :	0 - 4 ns
pulse-time :	20-25 ns
Without rear mirror onset :	~ 0 ns
pulse-time :	30 ns

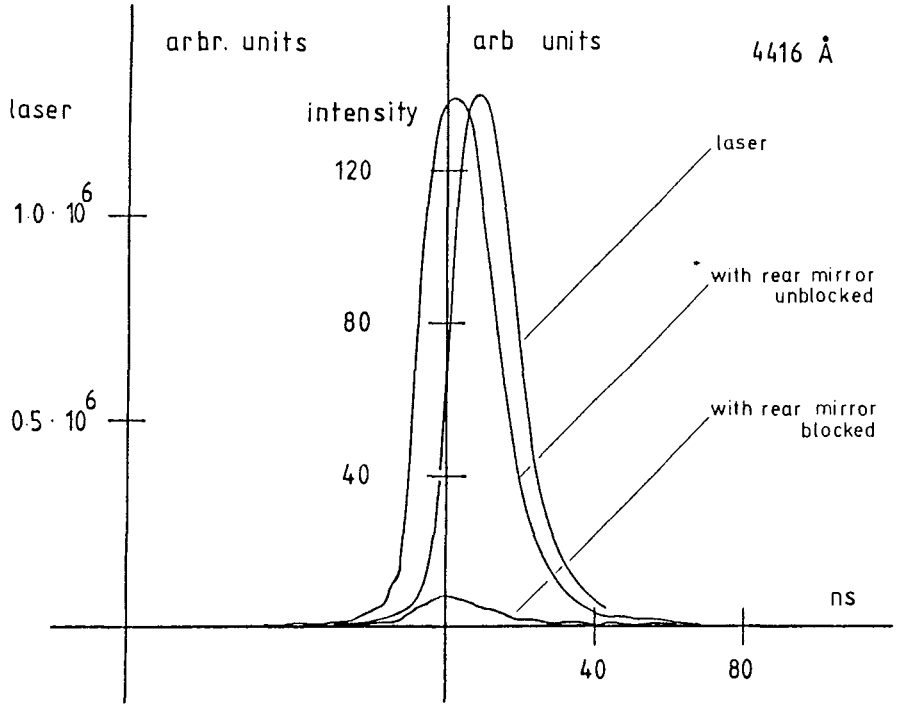

Fig 4.3.1 *Pulse shapes with and without rear mirror and for the laser pulse at 4416 Å. It should be noted that the laser intensity is in the order of 10,000 times stronger than that of blocked/ unblocked operation.*

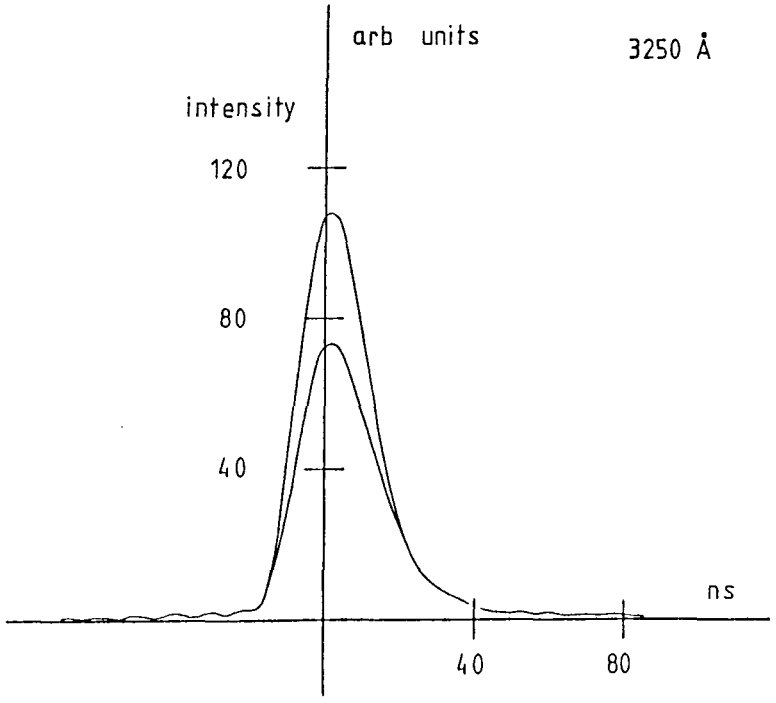

Fig 4.3.2 *Pulse shapes with and without rear mirror at 3250 Å.*

APPENDICES

A 1 THE GEOMETRICAL FACTOR IN GAIN CALCULATIONS FROM MIRROR TECHNIQUE

When calculating the gain of stimulated radiation one has to consider the geometrical configuration of the experimental set-up as a crucial factor in the evaluation process .

First let us look at some definitions:

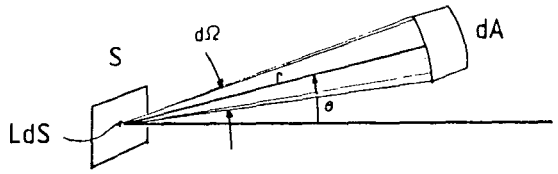

$d^2\Phi = LdS\cos\theta\, d\Omega$

$L_\theta = L$

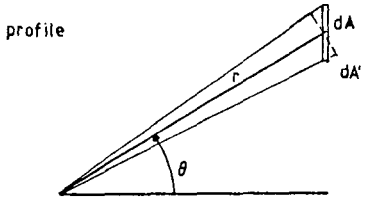

dA should be replaced by dA'

Fig a 1.1 a) Geometrical definition of terms used to calculate the geometrical factor. dA' = dA cosθ.

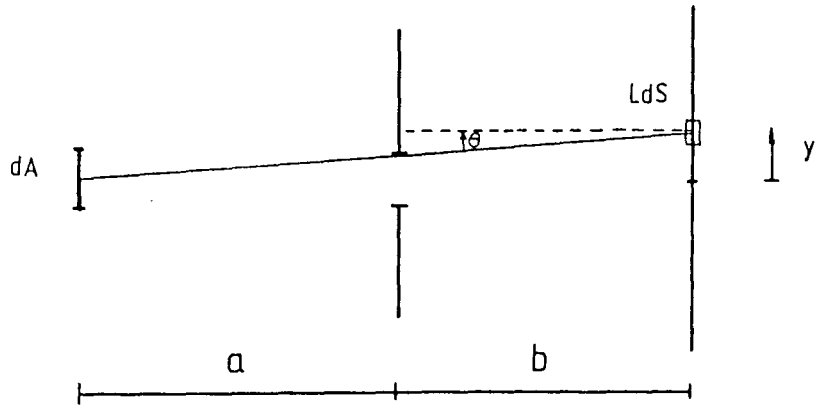

$$dS = 2\pi y\, dy$$

$$d\Omega = \frac{dA\cos\theta}{(a+b)^2 + y^2} \qquad d^2\Phi = \frac{L\cos^2\theta\, dA}{(a+b)^2 + y^2}\, 2\pi y\, dy$$

Fig A 1.1 b) Geometrical configuration of the experimental set-up without rear mirror. a = distance detektor - nearest diaphragm. b = distance diaphragm - cross section of the the active volume. y = distance from the centre of the active volume. L dS = circular cross section element.

Φ = radiant power (W)
L = radiance ($Wm^{-2}sr^{-1}$)
dA = surface element (m^2)
$d\Omega$ = element of solid angle (sr)

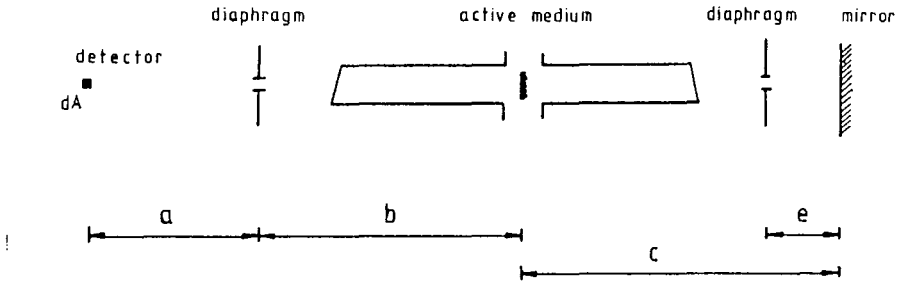

Fig A 1.2 a) *Geometrical configuration of the experimental set-up with rear mirror.*

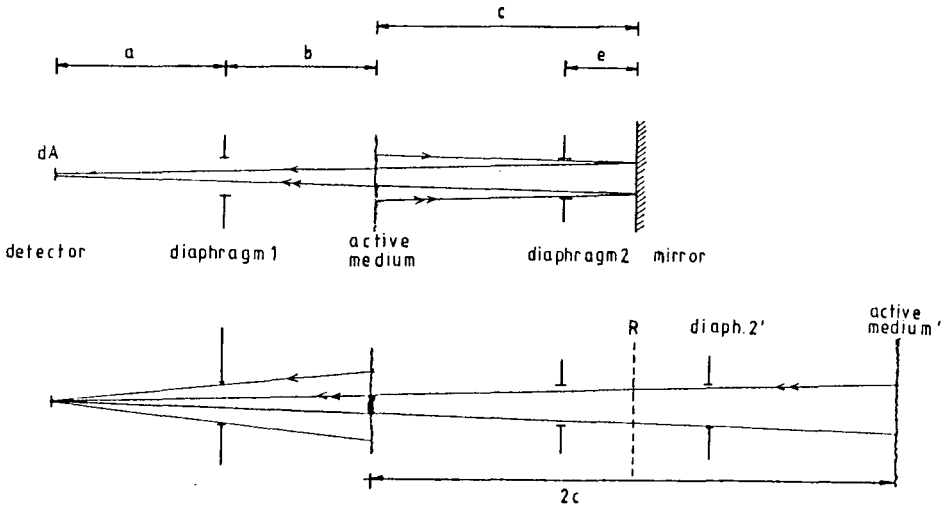

Fig A 1.2 b) *Primed terms represent mirror images.*

In our calculations we assume the detector to be point- like.
the source to be Lambertian.
d = the radius of the diaphragm (1 mm)

Using the labels in the above figure we get the following expressions:

$$d\Omega = \frac{dA \cos\theta}{(a+b)^2 + y^2} \qquad dS = 2\pi y\, dy$$

$$d^2\Phi = \frac{L \cos^2\theta\, dA\, 2\pi y\, dy}{(a+b)^2 + y^2} \qquad \cos\theta = \frac{a+b}{((a+b)^2 + y^2)^2}$$

The radiant power element falling into the detector is $d^2\Phi$ multiplied with $\cos\theta$. We then get the expression which is used in the coming evaluation.

$$d^2\Phi = 2\pi L (a+b)^3 \frac{y}{[(a+b)^2 + y^2]^{2.5}} dA\, dy \qquad (A1.1)$$

First we calculate the contribution directly from the radiant source (not via the mirror).

$$d\Phi = 2\pi L (a+b)^3 dA \int_0^{d(a+b)/a} y/[(a+b)^2 + y^2]^{2.5}\, dy$$

$$d\Phi = 2\pi L (a+b)^3 dA \left[-\frac{2}{6} [(a+b)^2 + y^2]^{-1.5} \right]_0^{d(a+b)/a} =$$

$$= 2/3\ \pi L\, dA \left[(a+b)^{-3} - \left[(a+b)^2 + \frac{d^2}{a^2}(a+b)^2 \right]^{-1.5} \right]$$

$$= 2/3\ \pi L\, dA \left[1 - [(a^2 + d^2)/a^2]^{-1.5} \right] \qquad (A1.2)$$

Now we continue with the part of radiation reflected by the mirror: Compared to the first case calculated, the radiation now undergoes an amplification by the factor $\exp(Gl)$, G being the absorption coefficient and l the length of the active volume .There is also the reflectivity of the mirror R, which is to be taken as a transmission coefficient.

$$d^2\Phi = 2\pi L \cos^3\theta \frac{y}{(a+b+2c)^2 + y^2} dA\, dy\, R\, e^{Gl} \qquad (A1.3)$$

$$\cos\theta = \frac{a+b+2c}{[(a+b+2c)^2 + y^2]^{0.5}} \qquad (A1.4)$$

$$d^2\Phi = 2\pi L (a+b+2c)^3 \frac{y}{[(a+b+2c)^2 + y^2]^{2.5}} dA\, dy\, R\, e^{Gl} \qquad (A1.5)$$

Next step is to evaluate the integral of this differential expression:

We have the boundary conditions: $0 < y < d(a+b+2c) / (a+b+c+e)$

given by $y_0 = 0$

$y_1 = d(a+b+2c) / (a+b+c+e)$

$$d\Phi = 2Re^{Gl}\pi L\ (a+b+2c)^3\ dA \int_{y_0}^{y_1} y/\left[\ (a+b+2c)^2 + y^2\ \right]^{2.5}\ dy$$

$$= 2/3\ Re^{Gl}\pi L\ dA \left[\ 1\ - \left[\ 1 + d^2/\ (a+b+2c)^2\ \right]^{-1.5}\ \right] \qquad (\ A1.6\ )$$

For the case of simplicity we introduce some new labels :

$d\Phi 1$ = the " direct radiation " radiant power
$d\Phi 2$ = the " reflected radiation " radiant power
$d\Phi 3$ = the measured radiant power without the mirror
$d\Phi 4$ = the measured radiant power with the mirror

$$d\Phi 3 = d\Phi 1$$
$$d\Phi 4 = d\Phi 1 + d\Phi 2$$

$$d\Phi 4\ /\ d\Phi 3 = 1 + Re^{Gl}\ \frac{1 - \left[\ 1+ d^2/(a+b+c+e)^2\ \right]^{-1.5}}{1 - \left[\ 1 + d^2/a^2\ \right]^{-1.5}} \qquad (\ A1.7\ )$$

In our experimental set-up $d^2/(a+b+c+e)^2 << 1$ and $d^2/a^2 << 1$ implies the use of the Taylor approximation on the expression of $d\Phi 4/d\Phi 3$ to the first degree :

$$1 - \left[\ 1 + d^2/(a+b+c+e)^2\ \right]^{-1.5} \approx 3/2\ d^2/(a+b+c+e)^2$$

$$1 - \left[\ 1 + d^2/a^2\ \right]^{-1.5} \approx 3/2\ d^2/a^2$$

So we get finally :

$$e^{Gl} = 1/R\ (\ d\Phi 4/d\Phi 3 - 1\ )\left[\ 1 + \frac{b+c+e}{a}\ \right]^2$$

Example : In our calculations

a = 104 cm
b = 44 cm
c = 39 cm
e = 4 cm
R = 0.7

giving a geometrical factor of 3.39

A 2 THE CURVE-OF-GROWTH TECHNIQUE

The curve-of-growth technique is a method to determine either the f -value, also known as the oscillator strength, of an absorption line, or the density, N_i , of absorbing atoms. The dimensionless quantity f describes what fraction of the energy of the classical oscillator should be ascribed to a given transition. For transitions from an upper level k to a lower level i reference [10] defines the emission f-value, f_{ki}, by the relation

$$A_{ki} = -3\, f_{ki}\gamma \qquad \text{(A2.1)}$$

where A_{ki} is the spontaneous emission probability and γ is the classical spontaneous emission or radiative decay rate.

$$\gamma = (e^2\omega^2)/(6\pi\varepsilon_0 mc^3) \qquad \text{(A2.2)}$$

where

e = the elementary charge
ω = the angular frequency of the radiation
ε_0 = the permittivity of free space
m = the electron rest mass
c = the speed of light.

The absorption f-value, f_{ik}, for an upward transition from level i to level k is defined by

$$g_i\, f_{ik} = -\, g_k\, f_{ki} \equiv g_f \qquad \text{(A2.3)}$$

where g_i and g_k are the statistical weights of the levels. Equations (A2.1) , (A2.2) and (A2.3) lead to an explicit expression for the transiton probability A_{ki} in terms of the absorption oscillator strength:

$$A_{ki} = [\ (e^2\omega_{ki}^2\ )/(2\pi\varepsilon_0 mc^3)\ ]\ [f_{ik}(g_i/g_k)] \qquad \text{(A2.4)}$$

The intensity of radiation of angular frequency ω transmitted by a column of absorbing gas with uniform density and temperature is given as

$$I_\omega(L) = I_\omega(0)\ \exp(-GL) \qquad \text{(A2.5)}$$

where G is the absorption coefficient. If the incident radiation comes from a source that keeps $I_\omega(0)$ esentially constant in the region of an absorption line, the transmitted intensity will have a dip centered on ω_{ki} and the spectral line is observed in absorption as shown in fig (A2.1).

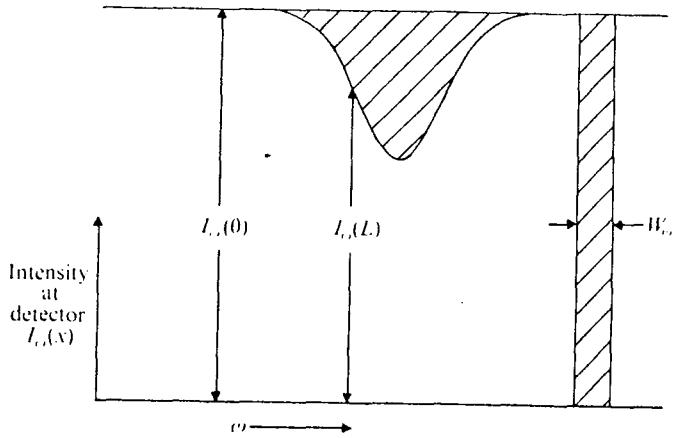

FIG A2.1 Definition of the equivalent width of an absorption line W_ω, in angular frequency units. The areas of the shaded sections are equal. (From ref 10)

In ref [10] the equivalent width, W_ω, of an absorption line is defined as the width of a rectangular strip of height $I_\omega(0)$ which has the same area as that of the absorption line, (see fig (A2.1)). This leads to the expression:

$$W_\omega \, I_\omega(0) = \int [I_\omega(0) - I_\omega(L)] \, d\omega \qquad (A2.6)$$

where the integral is taken over the profile of the absorption line. Equation (A2.6) can be rewritten as

$$W_\omega = \int [1 - I_\omega(L)/I_\omega(0)] \, d\omega \qquad (A2.7)$$

where W_ω has units of angular frequency. The equivalent width can also be expressed in units of length as

$$W_\lambda = \int [1 - I_\lambda(L)/I_\lambda(0)] \, d\lambda = (\lambda^2_{ki}/2\pi c) \, W_\omega \qquad (A2.8)$$

where λ_{ki} is the wavelength of the absorption line. By substituting equation (A2.5) into equation (A2.7) we get the equivalent width in terms of the absorption coefficient as

$$W_\omega = \int [1 - \exp(-GL)] \, d\omega \qquad (A2.9)$$

Ref [10] defines the absorption coefficient as:

$$G = (h\omega/8\pi^2) \, B_{ik} \, N_i \, [1 - (g_i N_k / g_k N_i)] \, g(\omega) \qquad (A2.10)$$

where N_i and N_k are the atom densities of the levels, and B_{ik} is the Einstein coefficient of absorption when the radiation is expressed in terms of its intensity . Ref [10] shows that B can be written as:

$$B_{ik} = [(4\pi^3 e^2 f_{ik})/(\varepsilon_0 h \, m\omega_{ki} c)] \qquad (A2.11)$$

$g(\omega)$ in equation (A2.10) above is known as the normalized line shape factor. This is usually taken to be a Voigt function , i.e. the line profile has the form of a folding integral of the Lorentzian, due to natural or collision broadening , and Gaussian , due to Doppler-broadening, distributions:

$$I(\omega_0 - \omega, \Gamma/\Delta) = \int_0^\infty G(\omega_0' - \omega_0, \Delta) \, L(\omega - \omega_0', \Gamma) \, d\omega_0' \qquad (A2.12)$$

where

$$L(\omega-\omega_0',\Gamma) = (\Gamma/2\pi)/[(\omega-\omega_0')^2 + \Gamma^2/4] \qquad (A2.13)$$

is the Lorentz function that shows the distribution of frequencies ω around the centre frequency ω_0', and

$$G(\omega_0'-\omega_0,\Delta) = [2/\Delta\sqrt{\pi}] \exp[-4(\omega_0'-\omega_0)^2/\Delta^2] \qquad (A2.14)$$

is the Gaussian function. Γ is the full width of the Lorentzian distribution at half intensity, and it is given as:

$$\Gamma = \gamma + 2N\sigma v \qquad (A2.15)$$

where N is the density of atoms, $v=[\ 8\ kT\ (M_1+M_2)/\pi M_1M_2\ ]^{0.5}$ is the mean relative velocity and σ is the collision cross-section. The full width of the Gaussian distribution at half intensity is given by:

$$\Delta\omega_{0.5}(\text{Doppler}) = \Delta(\ln 2)^{0.5} \qquad (A2.16)$$

where the linewidth parameter Δ is given by:

$$\Delta = 2(\omega_0/c)\ (2kT/M)^{0.5} \qquad (A2.17)$$

If we have a column of absorbing gas in which the optical depth at the centre of the line is small compared to unity, $GL\ll 1$, i.e. an optically thin sample, the exponential factor in equation (A2.9) may be expanded, and for a good approximation we have:

$$W_\omega = \int GL\ d\omega =$$
$$= (h\omega_{ki}/8\pi^2)\ B_{ik}\ N_i\ L\ [1-(g_iN_k/g_kN_i)] \int g(\omega)\ d\omega \qquad (A2.18)$$

Since the lineshape function $g(\omega)$ is normalized the integral in equation (A2.18) is equal to unity. Also at all temperatures attainable in the laboratory and for most transitions in the visible region, the ratio of upper to lower state populations in thermal equilibrium satisfies

$$g_iN_k/g_kN_i = \exp(-\ h\omega_{ki}/2\pi kT) \ll 1 \qquad (A2.19)$$

Equation (A2.18) is thus reduced to

$$W_\omega = (h\omega_{ki}/8\pi^2)\ B_{ik}\ N_i\ L \qquad (A2.20)$$

If the absorption f-value for the transition is introduced , we get using equation (A2.11):

$$W_\omega = (\pi e^2/2\varepsilon_0 mc)\ f_{ik}\ N_i\ L \qquad (A2.21)$$

Thus we can see that in the case of an optically thin sample the f-value of an absorption line can be obtained directly from measurement of the equivalent width, provided that the density of absorbing atoms, N_i , is known. Alternatively, if the f-value of a line is known, a measurement of W_ω enables us to determine N_i.

In case that the approximation GL << 1 is no longer valid, i.e. for an optically thick sample, the complete expression for the equivalent width, equation (A2.9), must be used. As can be seen from equation (A2.10), the frequency dependence of the absorption coefficient is given by the normalized line shape $g(\omega)$. This however, is usually taken to be a Voigt function. The shape of the Voigt profile depends on the ratio of the Lorentzian to the Gaussian linewidth parameters, Γ/Δ, which is not usually accurately known. This makes it difficult to determine the oscillator strength of an absorption line directly from a measurement of its equivalent width. One way to solve the problem is to measure the values of W_ω as a function of the density, N_i, of atoms in the absorbing gas. A graph of log W_ω is then plotted against log N_i. This is known as a curve of growth. With the use of different parameters $\alpha = 2\Gamma/\Delta$, theoretical curves of growth are also plotted by evaluating equation (A2.9), as shown in fig (A2.2).

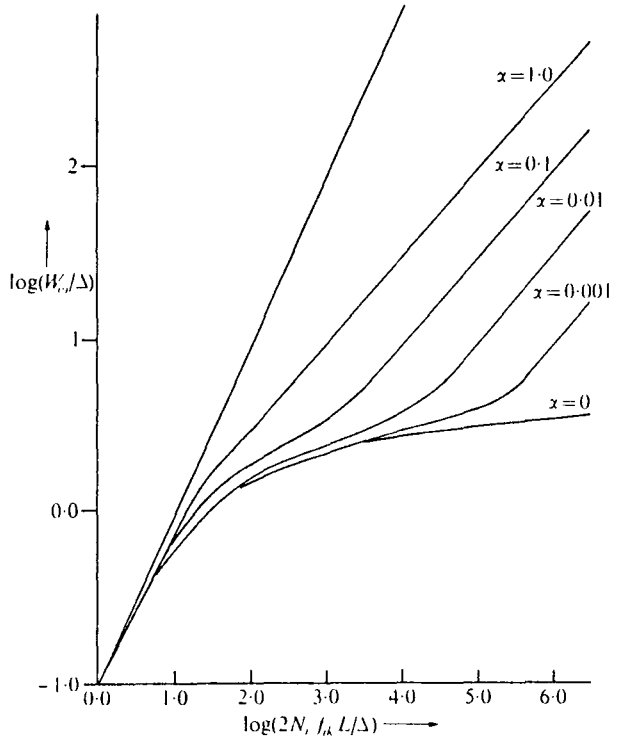

FIG A2.2 Theoretical curves of growth for different values of $\alpha = 2\Gamma/\Delta$. *(From ref 10)*

At low densities the equivalent width is proportional to N_i, (equation (A2.21)) , when N_i increases the curve of growth flattens out and eventually at high densities it can be shown that

$$W_\omega = \left[(\pi e^2 f_{ik} N_i L \Gamma)/(\varepsilon_0 mc)\right]^{0.5} \qquad \text{(A2.22)}$$

If the theoretical and experimental curves of growth are compared, the best values of Γ/Δ and f_{ik} can be obtained.

A 3 DENSITY VERSUS TEMPERATURE

A study of the results shows that the medium must be treated as an optically thick sample for all temperatures in this series of measurements. This means that equation (A2.22) must be applied. If equation (A2.8) is substituted into equation (A2.22) and the whole expression is squared, it gives:

$$W^2_\lambda = \left[(e^2 f_{ik} L \lambda^4_{ki})/(4\pi \varepsilon_0 mc^3)\right] N_i \Gamma \qquad (A3.1)$$

The length of the active volume L was put to 25 cm, and the approximation that the temperature is constant within the active volume was made. For the transition $5s5p\ ^1P_1 - 5s^2\ ^1S_0$ the lifetime is $\tau = 1.65$ ns [ref 11], $g_i = 1$, $g_k = 3$. With the use of equation (A2.4) and the fact that

$$A_{ki} = 1/\tau \qquad (A3.2)$$

we get

$$f_{ik} = \left[(g_k/g_i)\ (2\pi\varepsilon_0 mc^3/e^2\omega^2_{ki})\ (1/\tau)\right] \qquad (A3.3)$$

which gives an oscillator strength of $f_{ik} = 1.4292$ for the transition $5s5p\ ^1P_1 - 5s^2\ ^1S_0$. Likewise for the transition $5s5p\ ^3P_1 - 5s^2\ ^1S_0$: $f_{ik} = 4.667 \cdot 10^{-4}$. According to equation (A2.14) the Lorenz width is given by $\Gamma = \gamma + 2N\sigma v$, where $\gamma = 1/\tau$. With the use of $\sigma = 5 \cdot 10^{-15}$ cm^2 and v as defined in appendix 2 we get for the transition $5s5p\ ^1P_1 - 5s^2\ ^1S_0$: $\Gamma = 6.0606 \cdot 10^8 + 1.9410 \cdot 10^{-17} N T^{0.5}$, and likewise for the transition $5s5p\ ^3P_1 - 5s^2\ ^1S_0$: $\Gamma = 2.9232 \cdot 10^5 + 1.9410 \cdot 10^{-17}\ N\ T^{0.5}$. Since the equivalent widths could be determined from the absorption profiles, the atom densities could easily be determined from equation (A3.1). The resulting atom densities were then calibrated with the temperature and the measured gain plotted versus the atomic densities (fig 4.1.5). We made our calculations primary from the 2289 Å absorption and used the 3262 Å as a means of checking the validity of our calculations.We got the following results at 2289 Å :

Temperature [°C]	Eq.Width [Å]	Atomic density [10^{22} m^{-3}]
440	3.19	1.80
444	3.37	2.00
451	3.75	2.47
459	4.03	2.84
469	6.40	6.93
478	5.81	5.76
488	6.27	6.66

495	7.54	9.41
507	8.49	11.70
512	9.13	13.35
520	9.74	14.99
527	11.02	18.63
533	12.40	22.83
537	11.54	20.17
539	10.26	16.42

Many of the calculations acquire the density at 500^{0}C which we have given as $10 \cdot 10^{22}$ m^{-3}. Check with the 3262 Å absorption gave an eq.linewidth of 1.612 10^{-2} Å at 429 ^{0}C and an atomic density of $1.14 \cdot 10^{22}$ m^{-3}, which is fully in accordance with the results in the table above.

A 4 THE PHOTOIONIZATION PUMPING RATE

In the process of evaluating the intensity of excitation within the active volume we need to know the mechanisms inducing the emission of radiation from the Tungsten target.However if we assume the target to be a "gray" body in thermodynamic balance with the radiation impinging on its surface, the calculations could be very much simplified. An important factor is then the conversion coefficient for the W- target radiated by the Nd:YAG at the given temperature of the plasma. This gave us some problems since we did not know the necessary parameters, so we took another way. From the work done by H. Lundberg et. al [ref 2] we knew the peak temperature of the blackbody which coincides with the peak of the photoionizaton cross section at 30 nm to be of 12 eV.

Using Wiens' law $T \lambda' = 2898$ Kμm

λ' = peak value - wavelength of the blackbody radiation
T = temperature of the blackbody

we get for λ'=30 nm, T = 96 600 K. The intensity of 1.06 μm Nd:YAG radiation on the W- surface is 1.203 10^{15} Wm^{-2} given from the calculations below:

The divergence of the 1.06 μm radiation = θ = 280 μ rad
The optimal distance of the lens - target = d = 41 cm
The radius of the spot = r

$$r = d\theta = 115\ \mu m \qquad I = \frac{50\ MW}{\pi r^2} = 1.21\ 10^{15}\ Wm^{-2}$$

The conversion coefficient can be deduced from $I = \sigma T^4$ where σ = 5.67 10^{-8} Wm^{-2} K^{-4} and T = 96 600 K.

The conversion coeff. $k = \sigma T^4 / I_0$

$I_0 = 1.21\ 10^{15}\ Wm^{-2}$

This gives k = 0.0041 which is low but still leads to good results as we shall see further ahead. The number of ionizations taking place may be expressed by the density number $dN(\lambda) = \sigma(\lambda)N\ dx$, in the wavelength region of $[\lambda, \lambda+d\lambda]$. $\sigma(\lambda)$ is the corresponding cross section and N is the total density of non- ionized Cadmium atoms. Before we go any further we need some data in the table below :

Wavelength [Å]	Intensity (Plancks' rad.) $[Wm^{-2}]$	cross section [M barns]
100	$2.0067\ 10^{9}$	0
150	$3.7993\ 10^{10}$	1.9
200	$1.0816\ 10^{11}$	5.5
250	$1.5765\ 10^{11}$	14.7
300	$1.7188\ 10^{11}$	15.5
350	$1.6289\ 10^{11}$	14.7
400	$1.4372\ 10^{11}$	9.8
450	$1.2220\ 10^{11}$	7.4
500	$1.0201\ 10^{11}$	6.0
550	$8.4460\ 10^{10}$	4.5
600	$6.9775\ 10^{10}$	3.4
650	$5.7714\ 10^{10}$	2.8
	$\Sigma\ 1.2184\ 10^{12}$	

The intensities above are calculated from

$$I(\lambda) = \frac{2hc^2}{\lambda^5} \quad \frac{1}{\exp\,(hc/kT\lambda) \;-\; 1} \quad d\lambda$$

$$I(\text{table}) = \frac{1.1926\ 10^{-16}}{\lambda^5 \quad \exp\,(1.4905\ 10^{-7}/\ \lambda) \;-\; 1} \quad \Delta\ \lambda \quad W/m^2$$

$\Delta\ \lambda = 50\ 10^{-10}$ m

T = Plasma temperature 96 600 K

We now proceed with the calculation of the absorption in the active volume.In order to simplify the calculations an iterative method is used.The active volume is assumed here to have a rectangular cross section and was divided into segments of 1mm in the direction of the laser (see fig A 4.1).

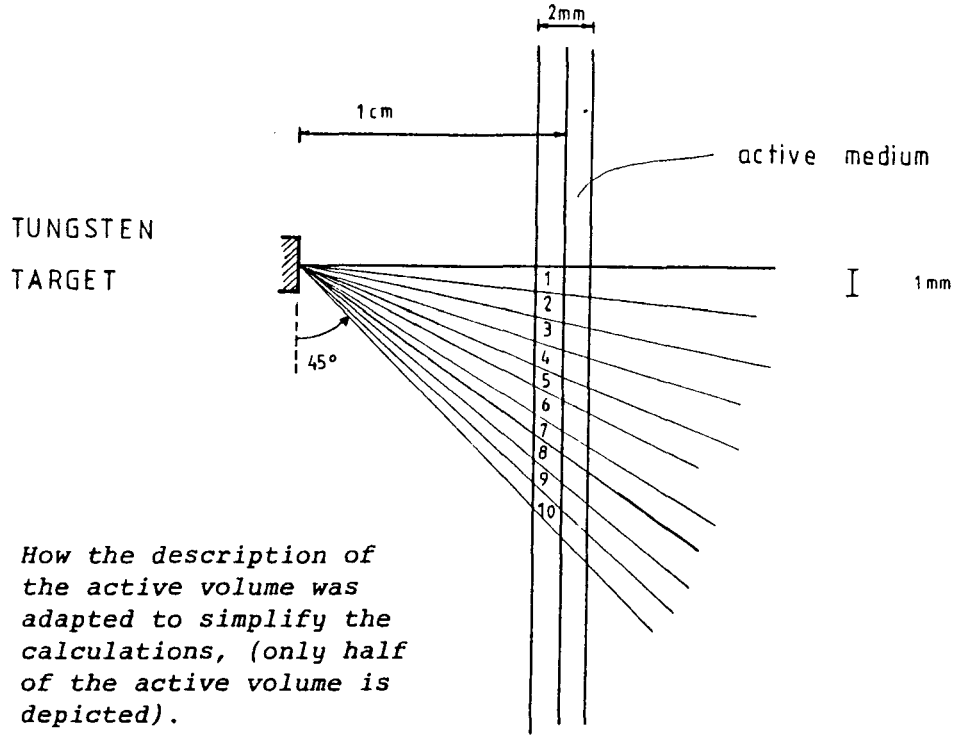

FIG A 4.1 *How the description of the active volume was adapted to simplify the calculations, (only half of the active volume is depicted).*

The spot of emission on the W- target is $dS = \pi(115\ 10^{-6})^2 = 4.15\ 10^{-8}\ m^2$ and the radiation is emitted within an angle of 45^0. From the description of the figure above we introduce some labels.

λ = wavelength
$\sigma(\lambda)$ = cross section of ionization
N = density of un ionized Cd atoms
c = speed of light
h = Plancks' constant
$L(\lambda)$ = radiated effect from the W- target

$$y(x) = 0.001 - 0.0005 \qquad x = 1,10$$

$$z(x) = (0.01)^2 + y^2(x) \qquad x = 1,10$$

$$\cos\theta = 0.01/\sqrt{z(x)} \qquad d\Omega = \frac{0.001 \cdot 0.002}{z(x)} \frac{0.01}{\sqrt{z(x)}} =$$

$$= 2\ 10^{-8}/\ (z(x))^{1.5}$$

The absorbed radiation in the active volume is :

$$d^2\Phi(\lambda) = L(\lambda)\, dS\; 2\sum_1^{10} \Big[e^{-N\sigma(\lambda)\, 0.009\, \sqrt{z}/\, 0.01} \cdot \Big\{ 1 - e^{-N\sigma(\lambda)\, 0.002\, \sqrt{z}/\, 0.01} \Big\} \cdot \cdot\; 0.01 \cdot 2\; 10^{-8} / (\sqrt{z}\; z^{1.5}) \Big] =$$

$$= 4\; 10^{-10}\, dS\, L(\lambda) \sum_1^{10} \Big[e^{-\,0.9\, N\, \sigma(\lambda)\, \sqrt{z}} \Big\{ 1 - e^{-\,0.2\, N\, \sigma(\lambda)} \Big\} / z^2 \Big]$$

The number of excitations per time unit then becomes :

$$dN/dt = \frac{4\; 10^{-10}\, L(\lambda)\, \lambda \cdot 4.1548\; 10^{-8}}{hc} \sum_1^{10} [\quad] =$$

$$= 8.3610\; 10^{8}\, L(\lambda)\, \lambda \sum_1^{10} [\quad] \qquad m^{-3}s^{-1}$$

The average number of excited atoms within the active volume is approximately dN/dt · τ. Here τ is the duration of the black body radiation, estimated to 50 ns. We then get the following results:

Wavelength [Å]	Number of exc. atoms
150	$4.127\; 10^{9}$
200	$3.047\; 10^{10}$
250	$5.421\; 10^{10}$
300	$6.855\; 10^{10}$
350	$7.842\; 10^{10}$
400	$8.928\; 10^{10}$
450	$8.456\; 10^{10}$
500	$7.418\; 10^{10}$
550	$5.978\; 10^{10}$
600	$4.596\; 10^{10}$
650	$3.624\; 10^{10}$
Σ	$6.265\; 10^{11}$

The active volume is $0.2 \cdot 0.2 \cdot 2 = 0.080\ cm^2$. The average density becomes then $7.8\; 10^{12}\ cm^{-3}$.

The statistical ratio between the two levels $^2D_{5/2}$ and $^2D_{3/2}$ should be 3:2 but as it is explained in the chapter of Photoionization it turns out to be 1.6 - 1.7 : 1 .

The upper level gets a density of $1/(1+1.7) * 7.8\ 10^{12}\ cm^{-3} = 2.9\ 10^{12}\ cm^{-3}$

The lower " " " $1.7/(1+1.7) * 7.8\ 10^{12}\ cm^{-3} = 4.9\ 10^{12}\ cm^{-3}$

The corresponding energy stored is :

Upper level $2.9\ 10^{12}\ hc/\ 3250\ 10^{-10} = 1.8\ \mu$ Joule cm^{-3}

Lower level $4.9\ 10^{12}\ hc/\ 4416\ 10^{-10} = 2.2\ \mu$ Joule cm^{-3}

This should be compared with our experimental result for 4416 Å : $= 1.97\ \mu$ Joule , with fully open diaphragms, and an active vol. of about 1 cc.

The 3250 Å however gave very little gain and was hidden in too much noice to be accepted .

A 5 ATOMIC DENSITY DERIVED FROM CALCULATIONS ON THE GAIN

The gain can be used to determine the density of atoms in the excited state. One problem is to find the correct emission profile. The contribution from isotope shift is prominent and the number of atoms of different isotopes is large. The only way for us to solve the problem was to ignore contribution from less frequent isotopes. It can be shown that only the two isotopes of Cd^{112} and Cd^{114} have any major influence on the profile. The folding integral between the homogeneous and inhomogeneous line broadening becomes the sum of the Doppler profiles, if we take the contributions from the homogeneous parts as Dirac profiles. For isotope shifts see ref [12].

The Dopplerprofile :

$$g(\Delta\omega) = \frac{c}{\omega_0}\left[\frac{M}{2\pi kT}\right]^{0.5} \exp - \left[\frac{Mc^2\,[\omega_0-\omega_0']^2}{2kT\,\omega_0^2}\right]$$

$$\Delta\omega = \omega_0-\omega_0'$$

Full width at half-maximum :

$$\Delta\omega(d) = 2\omega_0\left[\,2kT\ \ln 2\ /\ Mc^2\right]^{0.5}$$

ω_0 = centre frequency
ω_0' = actual frequency

M = mass of the isotope
k = Boltzmanns' constant
T = abs. temperature
c = speed of light

We then have :

$\Delta\omega(d)^{112} = 8.0229\ 10^9$ rad/s
$\Delta\omega(d)^{114} = 7.9591\ 10^9$ rad/s
isotope shift = $1.4641\ 10^9$ rad/s
rel. number of isotopes = % Cd^{112} = 24.07
% Cd^{114} = 28.86

From ref [13] we get :

$$W = \frac{4\pi^3}{3n^2 \varepsilon_0 c_0 h^2} |\mu|^2 I\, g_t(\omega-\omega_0)$$

$$W = 4\pi^2 \sigma I / h\omega \qquad \sigma = W/I \; h\omega/2\pi$$

$$A = 2\,\frac{n\,\omega_0^3 |\mu|^2}{3\,h\varepsilon_0\, c_0^3} \qquad |\mu|^2 = \frac{3\,A\,h\,\varepsilon_0\, c_0^3}{2\,n\,\omega_0^3}$$

$$\sigma = \frac{2\pi^2}{3n\,\varepsilon_0\, c_0\, h} |\mu|^2\, \omega\, g_t(\omega-\omega_0) =$$

$$= \frac{\pi^2 c_0^2 A}{n^2 \omega^2} g_t(\omega-\omega_0) \qquad (A5.1)$$

In terms of Wavelengths eq.(A5.1) becomes eq. (A5.2) :

$$\sigma = \frac{1}{4} A \lambda^2 g_t(\omega-\omega_0) \qquad (A5.2)$$

The gain G can be derived from eq. (A5.2). We consider the population inversion to be total i.e. the lower state to be empty.

So $G = \sigma N_2$ where N_2 is the upper level pop.

Thus $G = A/4 \cdot \lambda^2 g_t N_2$ (A5.3)

$$g_t = 0.939/\Delta\omega_{d,112} + 0.939/\Delta\omega_{d,114} =$$

$$= 6.222\ 10^{-11}\ s$$

From eq. (A5.3) we get :

$$N_2 = 4G / (A \lambda^2 g_t)$$

$$N_2 = 4G / A \lambda^2 g(\omega_C) = \underline{1.2\ 10^{14}\ cm^{-3}}$$

N_2 = density of exc. atoms
G = gain (5 cm^{-1})
λ = centre-wavelength (4416 Å)
A = Einstein coeff. for spont. emission (700 ns)

REFERENCES

1. S.P. Mc GLYNN, G.L. FINDLEY, R.H. HUEBNER "Photophysics and Photochemistry in the Vacuum Ultraviolet", NATO ASI series D.Reidel Publishing Company.

2. W.T. SILFVAST, O.R. WOOD, II, J.J. MACKLIN, H. LUNDBERG "Photoionization Lasers Pumped by Broadband Soft-X-Ray Radiation from Laser-Produced Plasmas", AIP Conference proceedings No. 119 Subseries on Optical Science and Engineering No. 5. "Laser Techniques in the Extreme Ultraviolet", Edited by S.E. Harris and T.B. Lucatorto, A.I.P. 1984.

3. W.T. SILFVAST, J.J. MACKLIN, O.T. WOOD, II "High-Gain Inner-Shell Photoionization Laser in Cd Vapor Pumped by Soft X-Ray Radiation from a Laser-Produced Plasma Source", Opt.Lett. 8, 551 (1983)

4. M.CARDONA, L.LEY "Photoemission in solids 1" General Principles,Topics in Applied Physics vol. 26, Springer-verlag Berlin Heidelberg N.Y. 1978.

5. J.BERKOWITZ "Photoabsorption,Photoionization,and Photoelectron Spectroscopy", Academic Press 1979.

6. G.M. McLELLAN,P.H.Y. LEE, and G. CAPORASO "Z- Dependence of the Laser Intensity Threshold for Inhibited Electron Thermal Conduction", Phys.Rev.Letters,vol.44 10 (1980).

7. JOHN.F.READY "Effects of High Power Laser Radiation", Academic Press 1971.

8. H. NISHIMURA, F. MATSUOKA, M. YAGI, K. YAMADA, H. NIKI T. YAMANAKA, C. YAMANAKA "Studies on Radiation Conversion and Transport in a 0.53 μm Laser Produced Gold Plasma", "Low Energy Diagnostics - 1981", edited by D.Attwood and B.L.Henke , AIP, N.Y. 1981.

9. G. YALE EASTMAN "The Heat Pipe", Scientific American, 218,38 (1968)

10. A. CORNEY "Atomic and Laser Spectroscopy", Clarendon Press, Oxford 1977.

11. R. PEPPERL "Relaxation des 5^1P_1- Zustandes von Cadmium bei Stößen mit Edelgasatomen und Wasserstoffmolekülen", Z. Naturforschung 25 a.

12. H.G. KUHN, FRS. and S.A. RAMSDEN "Isotope Shifts and Hyperfine Structure in the Atomic Spectrum of Cadmium", Proc.Roy.Soc A 237 , 485 1956.

13. O. SVELTO "Principles of Lasers", second edition, Plenum Press 1982